Theoretical Investigation of Bridge Seismic Responses with Pounding under Near-Fault Vertical Ground Motions

by

Haibo Yang, Xiaochun Yin, Hong Hao and Kaiming Bi

Theoretical Investigation of Bridge Seismic Responses with Pounding under Near-Fault Vertical Ground Motions

Haibo Yang[1], Xiaochun Yin[1,*], Hong Hao[2] and Kaiming Bi [2]

[1]Department of Mechanics and Engineering Science, Nanjing University of Science and Technology, Nanjing 210094, China
[2]Department of Civil Engineering, Curtin University, Kent Street, Bentley WA 6102, Australia

Abstract: Vertical earthquake loading is normally regarded not as important as its horizontal components and are not explicitly considered in many seismic design codes. However, some previous severe near-fault earthquakes reveal that the vertical ground motion component can be much larger than the horizontal components and may cause serious damage to the bridge structures. This paper theoretically investigates the vertical pounding responses of a two-span continuous bridge subjected to the severe near-fault vertical ground motions. The bridge is simplified as a continuous beam-spring-rod model. The structural wave effect and the vertical pounding between the bridge girder and the supporting bearing are considered, and the theoretical solutions of bridge seismic responses are derived from the expansion of transient wave functions as a series of eigenfunctions. The effects of vertical earthquake and vertical pounding on the bridge bearing, girder and pier are investigated. The numerical results show that the severe vertical earthquake loading may cause the bridge girder to separate from the supporting bearing and hence result in vertical poundings between them when they are in contact again. These vertical poundings can significantly alter the seismic responses of the bridge structure and may cause severe damage to the bridge components such as bridge girder, supporting bearing and bridge pier. Neglecting the influence of vertical earthquake loading may lead to inaccurate estimation of seismic responses of bridge structures, especially when they are subjected to near-fault earthquake with relatively large vertical motion.

Key words: theoretical investigation, bridge, vertical earthquake ground motion, seismic response, pounding effect, bearing, girder, pier.

1. INTRODUCTION

It is generally believed that a large safety factor against gravity loads exists in properly engineered structures including bridges (Papazoglou and Elnashai 1996). Many previous far-field seismic records also reveal that the amplitude of vertical component of an earthquake ground motion is normally less than those of the horizontal components (Yang and Lee 2007). Owing to these reasons, many current seismic design codes do not explicitly consider the vertical earthquake ground motions. For example, vertical ground motion is considered as an equivalent static vertical load when the site peak ground acceleration (PGA) is larger than 0.6 g (Button *et al*. 2002); Canadian Highway Bridge Design Code takes into account the vertical earthquake ground motion in a simplified way by increasing or decreasing the dead load action in load combinations, irrespective of earthquake magnitude, epicentral distance and site soil conditions (Bozorgnia and Campbell 2004). When the effects of vertical earthquake ground motions are

explicitly considered in the design process, the vertical response spectrum is taken typically as 2/3 of the horizontal response spectrum for the entire period range of engineering interest as proposed by Newmark (Elnashai and Papazoglou 1996). However, analyses of strong motion data indicate that the ratio of vertical to horizontal component (V/H) is sensitive to the frequency content of the seismic wave and distance from the epicentre. The ratios are normally larger for high frequency contents at short epicentral distances and smaller for low frequency contents at longer distances. It has been observed that in the ground motions generated from near-field earthquakes, the vertical to horizontal (V/H) ratio often exceeds unity, i.e. the vertical component is greater than the horizontal components. For example, in the 1994 Northridge earthquake, some recorded vertical acceleration was 1.18 g, and the V/H peak acceleration ratio was as high as 1.79 (Papazoglou and Elnashai 1996). In the 1995 Kobe earthquake, the peak of the vertical ground acceleration could be twice as high as that of the horizontal acceleration (Yang and Lee 2007). In the 1999 Chi-Chi earthquake, the PGA of vertical acceleration at station TCU068 reached 0.519 g, while in the two horizontal directions, the PGAs were 0.364 g and 0.501 g only (Wang et al. 2002). In the near-fault region (within rupture distance of 20 km) of the 2008 Wenchuan earthquake, the average and the maximum value of V/H were 0.89 and 1.20, respectively (Wang and Xie 2009).

Many numerical and experimental studies have been carried out to investigate the influence of vertical ground motions on the seismic responses of bridge structures. Saadeghvaziri and Foutch (1991) studied the inelastic behavior of reinforced concrete columns under combined horizontal and vertical accelerations. It was found that varying axial force in the column could result in pinched hysteresis, which in turn caused larger horizontal displacements and fluctuation in the shear capacity of the column. Yu (1996) analyzed the forces in the piers of three overpasses based on the three-dimensional (3D) models by using the Sylmar Hospital (Northridge) records as inputs. It was found that the axial force and longitudinal moment could increase by 21% and 7% if vertical component was considered. Elnashai and Papazoglou (1996) reported analytical and field evidence of the damaging effect of vertical ground motions on buildings and highway bridge structures. They concluded that strong vertical motions induced significant fluctuations in axial forces leading to a reduction of the column shear capacity. Collier and Elnashai (2001) then proposed simple procedures for assessing the significance of vertical ground motions.

They suggested that the vertical component of ground motion should be considered in analysis when the proposed structure was sited within approximately 25 km of an earthquake source. Button et al. (2002) examined several parameters including ground motion and structural system characteristics through primarily linear dynamic analyses and recommended a re-examination of existing design guidelines. Kunnath et al. (2008) examined a two-span highway bridge with a double-column bent considering six different structural configurations. The vertical component of ground motion was found to cause significant amplification in axial force demands in columns and moment demands in girders at both the mid-span and the face of the bent cap. Moreover, the increase of girder moment due to vertical motion could make the demand exceed the capacity, hence failure would be expected. Legeron and Sheikh (2009) proposed a theoretical approach to calculate support reactions of bridges under vertical ground motion. Jonsson et al. (2010) investigated the seismic response of a base-isolated bridge subjected to strong near-fault ground motions. The study showed that the near-fault pulse dominated the bridge response and an improved design method was proposed to consider near-fault pulse. Kim et al. (2011a, b) performed analytical and experimental studies to examine the effect of vertical ground motion on RC bridge piers. They investigated RC bridge piers by sub-structured pseudo-dynamic tests with combined horizontal and vertical excitations and by cyclic tests with different constant axial load levels. It was found that RC structures subjected to simultaneous horizontal and vertical motions were more vulnerable than those subjected to horizontal ground motion only. Gulerce et al. (2012) described the development of the seismic demand models for assessing the need to consider vertical motions in seismic bridge design. It was concluded that the vertical ground motions had a significant effect on three engineering demand parameters (EDPs), i.e. the axial force demand in columns, positive and negative moment demands at the face of the bent cap and positive and negative moment demands at the middle of the span. Lee and Mosalam (2014) carried out shaking table tests on the reduced-scale bridge columns under combined horizontal and vertical ground motions. Test results indicated that tension in the column caused by vertical excitation had the potential to degrade its shear capacity.

For a bridge structure subjected to a near-fault earthquake, the bearings of the bridge might be damaged due to the large vertical excitations, which may result in the bridge girder being lift up from the supporting bearings and impacting the bearing when

the girder is in contact again with the bearing. A huge impact force may develop owing to the dropping of the bridge girder to the bearings. This vertical impact may result in damages to the bridge girder, supporting bearings and/or even piers. For example, Figure 1(a) shows the vertical pounding damages to piers in the 2011 Christchurch earthquake (Chouw and Hao 2012), and Figure 1(b) shows the very unusual fractures developed in a bearing of Nielsen Bridge during the 1995 great Hanshin-Awaji earthquake due to vertical pounding (Tanimura *et al*. 2002).

Previous studies on the pounding responses mainly focused on the adjacent buildings (e.g., Pant and Wijeyewickrema 2013). For bridge structures, poundings are normally assumed to occur along the longitudinal directions of the bridge decks (Bi *et al*. 2010, 2011, 2013; Bi and Hao 2013). Although the vertical poundings between the uplifted bridge girders and supporting bearings was reported (Tanimura *et al*. 2002, Chouw and Hao 2012) and observed in a number of earthquakes, no study that is devoted to analyzing the effects of vertical pounding between bridge girder and bearings on bridge responses can be found in the literature. It is necessary to investigate the effect of possible vertical pounding effect on bridge seismic responses under strong vertical earthquake motion.

This paper conducts a theoretical derivation to estimate the seismic responses of bridge structures under near-fault vertical earthquake ground excitation and investigate the effect of vertical pounding on bridge structural responses. A continuous Beam-Spring-Rod model is adopted to simulate the seismic response of bridge. The theoretical solution of seismic responses, considering the structural wave effect and the possible pounding effect, are derived by the expansion of transient wave functions in a series of eigenfunctions. The seismic responses of a bridge model under three typical near-fault vertical earthquake ground motions are calculated. The effect of vertical earthquake ground motion and vertical pounding on bridge bearing, girder and pier are investigated.

2. THEORETICAL MODEL AND SOLUTIONS
2.1. Theoretical Model and Equation of Motion
A two-span continuous bridge as shown in Figure 2 is adopted as an example in the present study. The length of each span is x_0 and the height of the pier is L. For the bridge girder, the cross-section area is A, the Young's modulus is E, the area moment of inertia is I and the mass density is ρ. The corresponding parameters for the pier are A_r, E_r and ρ_r respectively. The two ends of the bridge girder (points A and B in Figure 2) are simply supported, and the base of the pier is fixed. A one-sided vertical spring with the compressive stiffness K and zero tensile stiffness is used to approximately model the bearing support. The self-weight of the bridge girder is represented by a uniformly distributed load q. The vertical ground motion from near-fault earthquake is denoted as $B(t)$. It should be noted that the primary objective of this paper is to investigate the vertical pounding responses of bridge structures to vertical earthquake loadings, although the horizontal motions will cause bridge structures to vibrate and the responses induced by horizontal and vertical ground motions are coupled, for clear observations of the effects of vertical ground excitations, in this study only the vertical ground excitations are considered. Further
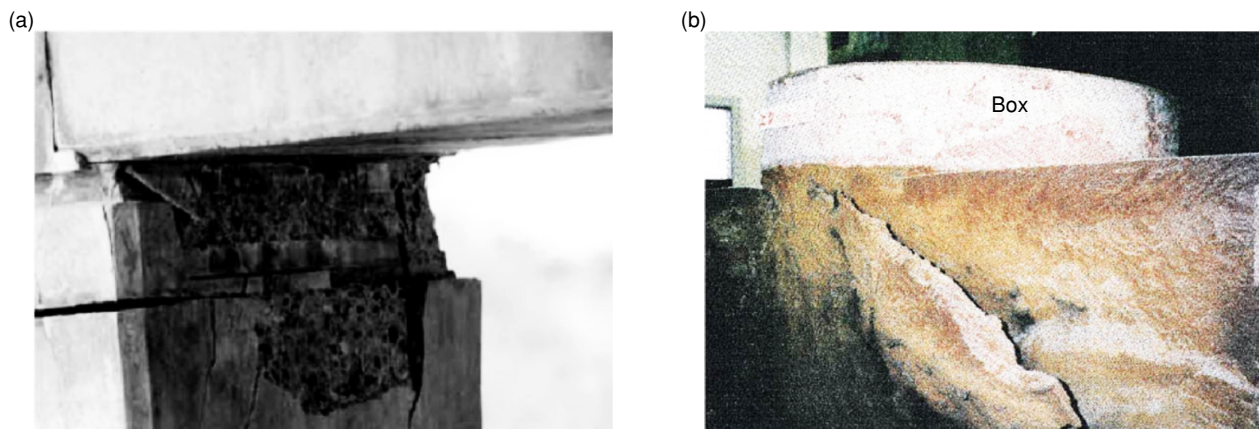
Figure 1. Typical vertical pounding induced damages in previous major earthquakes: (a) vertical pounding damage to bridge pier in the 2011 Christchurch earthquake (Chouw and Hao 2012); and (b) unusual fractures developed in a bridge bearing in the 1995 great Hanshin-Awaji earthquake (Tanimura *et al*. 2002)
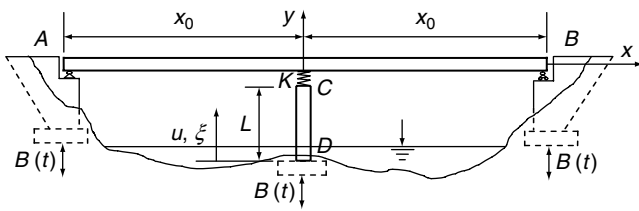
Figure 2. Schematic view of a two-span continuous bridge

study to investigate the coupled effects of horizontal and vertical ground motions on vertical pounding responses between bridge girders and supports is deemed necessary. Moreover, although damages to bridge pier and bearings owing to vertical poundings have been observed in previous earthquakes, to avoid further complicate the problem and allow the study concentrate on investigating the influences of vertical pounding on bridge responses, in the present study material nonlinearity is not considered.

In order to obtain the theoretical solution of seismic responses of bridge structures subjected to vertical earthquake loading, the vertical seismic excitation is expanded as the superposition of a series of harmonic components by the Fourier transformation as follows

$$B(t) = \sum_{m=1}^{N_0} B_m \sin\left(\omega_m t + \phi_m\right) \quad (1)$$

where B, ω and Φ are the ground displacement amplitude, circular frequency and phase angle of each component, N_0 is the number of frequency points required to well cover the frequency band of ground motions.

By assuming the bridge girder as a Bernoulli-Euler Beam and the pier as a St. Venant Rod, the equations of motion of the bridge shown in Figure 2 can be described as follows:

$$OA: \ \rho A \frac{\partial^2 y_1(x,t)}{\partial t^2} + EI \frac{\partial^4 y_1(x,t)}{\partial x^2} + q = 0$$

$$OB: \ \rho A \frac{\partial^2 y_2(x,t)}{\partial t^2} + EI \frac{\partial^4 y_2(x,t)}{\partial x^2} + q = 0 \quad (2)$$

$$CD: \ E_r A_r \frac{\partial^2 u(\xi,t)}{\partial \xi^2} - \rho_r A_r \frac{\partial^2 u(\xi,t)}{\partial t^2} = 0$$

In these equations, $y_i(x, t)$ ($i = 1, 2$) is the beam deflection and $u(\xi, t)$ is the longitudinal displacement of the rod. It should be noted that since Bernoulli-Euler Beam Theory and St. Venant Rod Theory are adopted in the derivations, the girder and pier considered in the present study need to be slender. Moreover, external damping and contact damping are not included in the model.

For the bridge shown in Figure 2, the two ends of the girder are simply supported and the pier is fixed, the boundary conditions are thus:

$$y_1(-x_0,t) = \sum_{m=1}^{N_0} B_m \sin\left(\omega_m t + \phi_m\right), \ \frac{\partial^2 y_1(-x_0,t)}{\partial x^2} = 0$$

$$y_2(x_0,t) = \sum_{m=1}^{N_0} B_m \sin\left(\omega_m t + \phi_m\right), \ \frac{\partial^2 y_2(x_0,t)}{\partial x^2} = 0 \quad (3)$$

$$u(0,t) = \sum_{m=1}^{N_0} B_m \sin\left(\omega_m t + \phi_m\right)$$

The continuity conditions of the beam in the middle section are:

$$y_1(0,t) = y_2(0,t), \ \frac{\partial y_1(0,t)}{\partial x} = \frac{\partial y_2(0,t)}{\partial x},$$

$$\frac{\partial^2 y_1(0,t)}{\partial x^2} = \frac{\partial^2 y_2(0,t)}{\partial x^2} \quad (4)$$

Strong vertical earthquake can lift up the bridge girder, resulting in it being separated from the bearing, but it will come back in contact with the supporting bearing again due to the gravity load as discussed above. This is a nonlinear process because separation and contacting changes the structural stiffness, which can be divided into two different phases, the in-contact phase and out-of-contact phase. In the present study, the in-contact phase and the out-of-contact phase are modelled by two linear elastic systems. Therefore the nonlinear pounding process is described by piecewise linear elastic responses solved in two systems. The change from one linear elastic system to another one is defined by the in-contact

condition and the out-of-contact condition. In each linear elastic system, the partial differential equation of motion (Eqn 2) can be solved by the superposition of linear harmonic motion.

For the in-contact case, the continuity conditions of displacement and shear force between the beam and the spring can be described as follows:

$$u(l,t) - y_1(0,t) = \delta = \frac{F}{K} = -\frac{E_r A_r}{K} \frac{\partial u(l,t)}{\partial \xi} \qquad \text{(5-a)}$$

$$EI(\frac{\partial^3 y_1(0,t)}{\partial x^3} - \frac{\partial^3 y_2(0,t)}{\partial x^3}) = E_r A_r \frac{\partial u(l,t)}{\partial \xi} \qquad \text{(5-b)}$$

where δ is the compression displacement of linear spring, and F is the bearing reaction force. For the out-of-contact case, the girder and pier vibrate separately. The contact force between the beam and the spring is zero. There is no additional continuity condition between the beam and the spring.

If uplifting occurs, pounding between girder and bearing will take place when the beam comes back in contact with the bearing again. Under strong vertical excitations with sufficient duration, multiple uplifting and pounding might occur, resulting in multiple separation and contacting phases to take place alternatively. The responses of bridges subjected to strong vertical earthquakes can be modelled as:

1) Pre-separation phase: in this phase the beam is supported by the bearing, beam and rod vibrate together as a whole system;

2) Separation phase: the beam is uplifted, and the beam and rod vibrate separately with their own natural frequencies ω_{bn} and ω_{rn}; and

3) Pounding phase: during this phase, the beam is in contact with the bearing again, and the continuity conditions in Eqn 5 is satisfied.

The initial displacements and velocities at different locations of the girder and pier in each of the three phases can be expressed in an analytical form. Particularly for the pre-separation phase, they are:

$$y_1(x,0) = \begin{bmatrix} q(-5x_0^4 + 6x^2 x_0^2 - x^4)\text{-} \\ 2F_s(2x_0^3 - x^3 - 3x^2 x_0) \end{bmatrix} / 24EI,$$

$$\frac{\partial y_1(x,0)}{\partial t} = 0$$

$$y_2(x,0) = \begin{bmatrix} q(-5x_0^4 + 6x^2 x_0^2 - x^4)\text{-} \\ 2F_s(2x_0^3 + x^3 - 3x^2 x_0) \end{bmatrix} / 24EI,$$

$$\frac{\partial y_2(x,0)}{\partial t} = 0 \qquad \text{(6)}$$

$$u(\xi,0) = F_s \xi / E_r A_r, \quad \frac{\partial u(\xi,0)}{\partial t} = 0$$

where F_s is the initial contact force between the girder and bearing, which can be expressed as:

$$F_s = -5qx_0^4 \big/ \left(24EIL \big/ E_r A_r + 24EI \big/ K + 4x_0^3\right) \qquad \text{(7)}$$

Different from the pre-separation phase, the initial conditions for the separation and contacting phases are the values corresponding to the end of the previous phase.

2.2. Solutions of Seismic Responses in the Pounding Phase

Modelling the multiple poundings between girder and bearing are not straightforward due to the existence of pounding-induced waves. Poundings will generate strong transient waves propagating in the beam and rod even they are separated again. The flexural waves travelling along the beam, and the longitudinal waves travelling along the rod will interact with each other at the contacting location during pounding and result in complex dynamic responses. In this section, the transient responses of bridge are solved by using the expansion of transient wave functions in a series of Eigenfunctions (i.e., wave modes) (Yin 1997; Yin and Wang 1999; Yin and Yue 2002; Yin *et al*. 2007).The fundamental form of the solutions contains two parts. In the pounding phase, the beam deflection and rod longitudinal displacement can be derived as

$$y_1(x,t) = y_{1s}(x,t) + \sum_{n=1}^{\infty} \phi_{nb1}(x)q_n(t)$$

$$y_2(x,t) = y_{2s}(x,t) + \sum_{n=1}^{\infty} \phi_{nb2}(x)q_n(t) \qquad \text{(8)}$$

$$u(\xi,t) = u_s(\xi,t) + \sum_{n=1}^{\infty} \phi_{nr}(\xi)q_n(t)$$

The first part of the expression is the quasi-static solution. The three quasi-static solutions satisfying inhomogeneous boundary conditions as listed in Eqns 4 and 5 are:

$$y_{1s}(x,t) = \left[\begin{array}{l} q(-5x_0^4 + 6x^2x_0^2 - x^4) + 2F(t) \\ (2x_0^3 - x^3 - 3x^2x_0) \end{array} \right] \Big/ 24EI +$$

$$\sum_{m=1}^{N_0} B_m \sin(\omega_m t + \phi_m)$$

$$y_{2s}(x,t) = \left[\begin{array}{l} q(-5x_0^4 + 6x^2x_0^2 - x^4) + \\ 2F(t)(2x_0^3 + x^3 - 3x^2x_0) \end{array} \right] \Big/ 24EI +$$

$$\sum_{m=1}^{N_0} B_m \sin(\omega_m t + \phi_m) \qquad (9)$$

$$u_s(\xi,t) = F(t)\xi / E_r A_r + \sum_{m=1}^{N_0} B_m \sin(\omega_m t + \phi_m)$$

The second part is the dynamic solution, which is the summation of modal responses with respect to the flexural wave modes ϕ_{nb1} and ϕ_{nb2} for the beam and longitudinal wave modes ϕ_{nr} for the rod and the corresponding time functions $q_n(t)$. The wave modes are governed by the Eigenvalue problem with the Eigenequations:

$$a^2 \frac{\partial^4 \phi_{nb1}}{\partial x^4} - \omega_n^2 \phi_{nb1} = 0, \quad a^2 \frac{\partial^4 \phi_{nb2}}{\partial x^4} - \omega_n^2 \phi_{nb2} = 0,$$

$$c_r^2 \frac{\partial^2 \phi_{nr}}{\partial x^2} + \omega_n^2 \phi_{nr} = 0 \qquad (10)$$

with homogenous boundary conditions:

$$\phi_{b1}(-x_0) = 0, \quad \phi_{b1}''(-x_0) = 0$$

$$\phi_{b2}(x_0) = 0, \quad \phi_{b2}''(x_0) = 0, \quad \phi_r(0) = 0$$

$$\phi_{b1}(0) = \phi_{b2}(0), \quad \phi_{b1}'(0) = \phi_{b2}'(0), \quad \phi_{b1}''(0) = \phi_{b2}''(0) \quad (11)$$

$$\phi_{b1}(0) = \phi_r(l) + \frac{E_S A_S \phi_r'(l)}{k}$$

$$EI(\phi_{b1}'''(0) - \phi_{b2}'''(0)) = E_S A_S \phi_r'(l)$$

where $a = \sqrt{EI / \rho A}$ Dis the coefficient related to the beam flexural wave speed and $c_r = \sqrt{E_r / \rho_r}$ F is the longitudinal wave speed in the rod. The flexural wave modes ϕ_{bn1} and ϕ_{bn2}, and longitudinal wave modes ϕ_{rn} can be expressed as

$$\phi_{bn1} = A_{n1} \sin k_{bn}x + B_{n1} \cos k_{bn}x$$
$$+ C_{n1} \sin h k_{bn}x + D_{n1} \cos h k_{bn}x$$

$$\phi_{bn2} = A_{n2} \sin k_{bn}x + B_{n2} \cos k_{bn}x$$
$$+ C_{n2} \sin h k_{bn}x + D_{n2} \cos h k_{bn}x \qquad (12)$$

$$\phi_{rn} = E_n \sin k_{rn}\xi + F_n \cos k_{rn}\xi$$

where k_{bn}, k_{bn}, k_{rn} are the wave numbers, and A_{n1}, B_{n1}, C_{n1}, D_{n1}, A_{n2}, B_{n2}, C_{n2}, D_{n2}, E_n, F_n are the coefficients of the beam and rod wave modes. The flexural and longitudinal wave modes satisfy the orthogonality conditions, which can be derived easily from the Eigenequations (Eqn 10) and the homogenous boundary conditions (Eqn 11):

$$\int_{-x_0}^{0} \rho \varphi_{b1i} \varphi_{b1j} A dx + \int_{0}^{x_0} \rho \varphi_{b2i} \varphi_{b2j} A dx$$

$$+ \int_{0}^{L} \rho_r \varphi_{ri} \varphi_{rj} A_r d\xi = \delta_{ij} \qquad (13)$$

where δ_{ij} is the Dirac function. Substituting wave mode functions into Eqn 10 yields a set of linear algebraic equations in a matrix form. The existence of non-trivial solutions leads to the determinant of the coefficient matrix being zero, which forms the beam-rod frequency equation as follows:

$$E_r A_r k_{rn} \cos k_{rn} L (\tan k_{bn}x_0 - \tan h k_{bn}x_0)$$

$$+ 4EIk_{bn}^3 (\sin k_{rn}L + \frac{E_r A_r k_{rn} \cos k_{rn}L}{K}) = 0 \qquad (14)$$

The coefficient of beam and rod wave modes can be determined by substituting Eqn 12 into Eqn 13. Then the beam and rod wave modes in Eqn 12 can be calculated. The expression of the Eigenfunctions can be given as:

$$\phi_{nb1} = M_n A_n \left(-\frac{\sin k_{bn}(x+x_0)}{\cos k_{bn}x_0} + \frac{\sinh k_{bn}(x+x_0)}{\cosh k_{bn}x_0} \right)$$

$$\phi_{nb2} = M_n A_n \left(\begin{array}{c} \dfrac{\sin k_{bn}(x-x_0)}{\cos k_{bn}x_0} \\ -\dfrac{\sinh k_{bn}(x-x_0)}{\cosh k_{bn}x_0} \end{array} \right) \qquad (15)$$

$$\phi_{nr} = A_n \sin k_{rn}\xi$$

$$M_n = \frac{\sin k_{rn}L + \dfrac{E_S A_S k_{rn}\cos k_{rn}L}{k}}{\left[\dfrac{\sinh k_{bn}x_0}{\cosh k_{bn}x_0} - \dfrac{\sin k_{bn}x_0}{\cos k_{bn}x_0} \right]} = \frac{E_S A_S k_{rn}\cos k_{rn}L}{4EIk_{bn}^3}$$

$$A_n^{-2} = M_{3n}^2 \rho A x_0 \left(\frac{\sin^2 k_{bn}x_0}{\cos^2 k_{bn}x_0} + \frac{\sinh^2 k_{bn}x_0}{\cosh^2 k_{bn}x_0} \right)$$

$$+ \frac{\rho_s A_s}{8k_{rn}}\sin 2k_{rn}l + \frac{3\rho_s E_s A_s^2 \cos^2 k_{rn}l}{4k} + \rho_s A_s \frac{l}{2}$$

The construction of the quasi-static part and the dynamic part makes the real boundary conditions be satisfied completely, but the boundary conditions in Eqn 3 need to be satisfied by further construction of the time functions $q_n(t)$. Substituting Eqn 6 into Eqn 1, and using the orthogonality conditions in Eqn 12, the following time differential equation can be obtained:

$$\ddot{q}_n(t^*) + \omega_n^2 q_n(t^*) = \ddot{Q}_n(t^*) \qquad (16)$$

where

$$Q_n(t^*) = -\int_{-x_0}^{0} \rho A \varphi_{bn1}(x) y_{1s}(x,t^*)dx$$

$$- \int_{0}^{x_0} \rho A \varphi_{bn2}(x) y_{2s}(x,t^*)dx$$

$$- \int_{0}^{L} \rho_r A_r \varphi_{rn}(x) u_s(\xi,t^*)d\xi$$

$t^* = t - t_{2k}$ is the time variable of the k-th pounding phase ($k = 0$ is the first pounding phase), t_{2k} is the initial time of the k-th pounding phase.

Using the Laplace transform, $q_n(t)$ then can be obtained as follows:

$$q_n(t^*) = q_n(0)\cos(\omega_n t^*) + \frac{1}{\omega_n}\dot{q}_n(0)\sin(\omega_n t^*)$$
$$+ \frac{1}{\omega_n}\int_{0}^{t^*}\ddot{Q}_n(t_{2k}+\tau)\sin(\omega_n(t^*-\tau))d\tau \qquad (17)$$

$$q_n(0) = \int_{-x_0}^{x_0}\rho A \varphi_{bn}(x)y_s(x,t_{2k}^-)dx +$$
$$\int_{0}^{L}\rho_r A_r \varphi_{rn}(x)u_s(\xi,t_{2k}^-)d\xi + Q_n(0)$$

$$\dot{q}_n(0) = \int_{-x_0}^{x_0}\rho A \varphi_{bn}(x)\dot{y}_s(x,t_{2k}^-)dx$$
$$+ \int_{0}^{L}\rho_r A_r \varphi_{rn}(x)\dot{u}_s(\xi,t_{2k}^-)d\xi + \dot{Q}_n(0)$$

where $y_s(x, t_{2k}^-)$ $\dot{y}_s(x, t_{2k}^-)$ and $u_s(\xi, t_{2k}^-)$ $\dot{u}_s(\xi, t_{2k}^-)$ are the initial displacement and velocity distributions which are the corresponding values at the end of the previous phase as mentioned above. The initial time of every pounding phase can be determined by the in-contact condition:

$$u(L,t) - y_1(0,t) - \frac{F(t)}{K} = 0 \qquad (18)$$

2.3. Solutions of Seismic Responses in the Separation Phase

In the separation phase, similar approaches to calculate the wave modes, frequencies, the coefficient of wave modes and time functions as in the pounding phase can be applied. Similar to Eqn 8, the beam deflection and rod longitudinal displacement can be expressed as:

$$y_b(x,t) = y_{bs}(x,t) + \sum_{m=1}^{\infty}\varphi_{bm}(x)q_{bm}(t) \qquad (19)$$

$$u_b(\xi,t) = u_{bs}(\xi,t) + \sum_{m=1}^{\infty} \varphi_{rm}(\xi) q_{rm}(t)$$

The two quasi-static solutions are:

$$y_{bs}(x,t) = q(-5x_0^4 + 6x^2 x_0^2 - x^4)$$
$$+ \sum_{m=1}^{N_0} B_m \sin(\omega_m t + \phi_m) \tag{20}$$

$$u_{bs}(\xi,t) = \sum_{m=1}^{N_0} B_m \sin(\omega_m t + \phi_m)$$

The beam and rod wave modes in the form of Eigenfunctions are:

$$\varphi_{bm}(x) = A_{bm} \sin \bar{k}_{bm}(x + x_0) \tag{21}$$

$$\varphi_{rm}(x) = A_{rm} \sin \bar{k}_{rm}\xi$$

The time functions can be obtained as follows:

$$q_{bm}(t^*) =$$
$$q_{bm}(0)\cos(\omega_{bm}t^*) + \frac{1}{\omega_{bm}}\dot{q}_{bm}(0)\sin(\omega_{bm}t^*)$$
$$+ \frac{1}{\omega_{bm}}\int_0^{t^*} \ddot{Q}_{bm}(t_{2k+1} + \tau)\sin(\omega_{bm} \cdot (t^* - \tau))d\tau \tag{22}$$

$$q_{rm}(t^*) = q_{rm}(0)\cos(\omega_{rm}t^*) + \frac{1}{\omega_{rm}}\dot{q}_{rm}(0)\sin(\omega_{rm}t^*)$$
$$+ \frac{1}{\omega_{rm}}\int_0^{t^*} \ddot{Q}_{rm}(t_{2k+1} + \tau)\sin(\omega_{rm} \cdot (t^* - \tau))d\tau$$

For the simply supported beam and fixed rod, the frequencies are

$$\bar{k}_{bm} = \sqrt{\omega_{bm}/a} = m\pi/2x_0,$$
$$\bar{k}_{rm} = \omega_{rm}/c_r = (2m-1)\pi/2L \tag{23}$$

Based on the orthogonality condition of wave mode functions, the beam and rod frequencies A_{bm} and A_{rm} can be calculated as:

$$A_{bm} = 1/\sqrt{\rho A x_0}, \quad A_{rm} = \sqrt{2/\rho_r A_r L},$$
$$m = 1, 2, 3, \dots\dots \tag{24}$$

where $t^* = t - t_{2k+1}$ is the time variable of the k-th separation phase ($k = 1$ is the first separation phase), t_{2k+1} is the initial time of the k-th separation phase, and $y_s(x, t_{2k+1}^-) \dot{y}_s(x, t_{2k+1}^-)$ and $u_s(\xi, t_{2k+1}^-)$ and $\dot{u}_s(\xi, t_{2k+1}^-)$ are the initial displacement and velocity distributions which again correspond to values at the end of previous phase. The initial time of every separation phase is determined by the out-of-contact condition:

$$F(t) = 0 \tag{25}$$

The time functions, $q_{bm}(t^*)$ and $q_{rm}(t^*)$, and their initial values, $q_{bm}(0)$, $q_{rm}(0)$, $\dot{q}_{bm}(0)$ and $\dot{q}_{rm}(0)$, have the same forms as those of $q_n(t^*)$, $q_n(0)$ and $\dot{q}_n(0)$. However, they have their own frequencies (ω_{bm} and ω_{rm}), initial displacement, velocity distributions and their own integral parts.

2.4. Solutions of the Multiple Pounding Force

During the pounding process, the pounding force F is generated between the girder and the bearing. Generally speaking, two kinds of techniques, the stereomechanical approach and the contact element approach, are used to model the pounding phenomena in bridge structures under earthquake excitations. The pounding forces obtained from these two models depend on the coefficient of restitution and the damping coefficient, but the selection of these coefficients is difficult since it depends on many factors. In this study, a new theoretical approach of determining the multiple vertical pounding forces is presented based on the transient internal force on the contact surface of the girder and bearing. In this new approach, there are two main steps to calculate the pounding force. First, the transient responses in the pounding phase are solved as in Section 2.2. Then, the internal forces, i.e. the internal stress at the pier end or the spring force are obtained and form the solution of the transient responses. The pounding force is calculated as follows:

$$F(t) = \begin{cases} \iint_{\Gamma_r} \sigma_r dA & t_{2k} \le t \le t_{2k+1} \\ 0 & t_{2k+1} \le t \le t_{2k+2} \end{cases} \quad \text{or} \tag{26}$$

$$F(t) = \begin{cases} K\big(u(L,t) - y_1(0,t)\big) & t_{2k} \le t \le t_{2k+1} \\ 0 & t_{2k+1} \le t \le t_{2k+2} \end{cases}$$

where σ_r is the internal stress at the pier end, and Γ_r is contact area at the pier end.

It is believed that this new approach on determining the pounding force has the following advantages. First, the pounding contact model is not used, and the coefficient of restitution and the damping coefficient are therefore not needed. Second, the result of the pounding force is more reliable since it is based the well-established theories for the transient wave propagation in the girder and the pier in Sections 2.2 and 2.3. Third, the time discretization method is avoided which can result in the divergence of pounding force in calculations (Wang and Kim 1996).

The similar method has been used successfully in solving the multiple-impact problems of two coaxial hollow cylinders (Yin 1997; Yin and Wang 1999; Yin and Yue 2002) and the repeated-impact problem between a cantilever beam and a rod (Yin *et al.* 2007).

3. BRIDGE MODEL

A typical highway bridge in China is used as an example in this section to illustrate the theoretical method proposed in Section 2. The bridge is a two-span continuous prestressed reinforced concrete box girder bridge. The single pier is composed of two circular concrete columns with longitudinal bars and spiral hoops. Figure 3(a) shows the cross section of the bridge at the centre of the pier, and Figure 3(b) shows the cross section of each column and the reinforcement details in the column. The corresponding parameters of the girder and pier are given in Table 1.

To simplify the analysis, the equivalent parameters of the bridge are used, which can be calculated based on the code for the design of highway reinforced concrete and prestressed concrete bridges and culverts in China. Based on the specifications, it can be calculated that the equivalent Young's modulus of the pier is $E_r = (E_c A_c + E_y A_y) / (A_c + A_y) = 31.7$ GPa, the equivalent section area of pier $A_r = A_c + (\alpha_y - 1) A_y = 3.228$ m^2, where $\alpha_y = E_y / E_c$ is the enhancement coefficients. The equivalent section area of the girder is $A = A_c + (\alpha_y - 1) A_y + (\alpha_p - 1) A_p = 6.4$ m^2. The equivalent moment of inertia of the girder is $I = I_c + I_y + I_p = 3.684$ m^4. The the equivalent flexural stiffness of the girder is $EI = 0.95E_c I = 1.21 \times 10^{11}$ N·m^2. The circular plate rubber bearing with the type of GYZ850 × 171 is placed between the girder and pier. The rubber bearing with long-narrow shape whose hysteresis curve can be considered to be a linear elastic spring. The vertical stiffness of rubber bearing is approximated as $K = 2 \times 10^9$ N/m. The total weight of bridge superstructure is 1948.34 tons

and the uniformly distributed loading is $q = 256360.53$ N/m.

4. VERTICAL EARTHQUAKE GROUND MOTIONS

Ground motions from three typical near-fault earthquakes as listed in Table 2 are selected as input in the present study to demonstrate the vertical pounding on bridge responses. Because ground displacement is used as input in the above derived solutions, the recorded ground displacement is expressed as the superposition of a series of the harmonic components as defined by Eqn 1. In the present study, the circular frequency, the amplitude and phase angle of each harmonic is determined from the Fourier transform of the ground displacement time history. To well represent the ground displacement time history, one hundred frequency points are used. As shown in Figure 4, the summation of 100 harmonics well represents the recorded vertical earthquake ground displacement time histories.
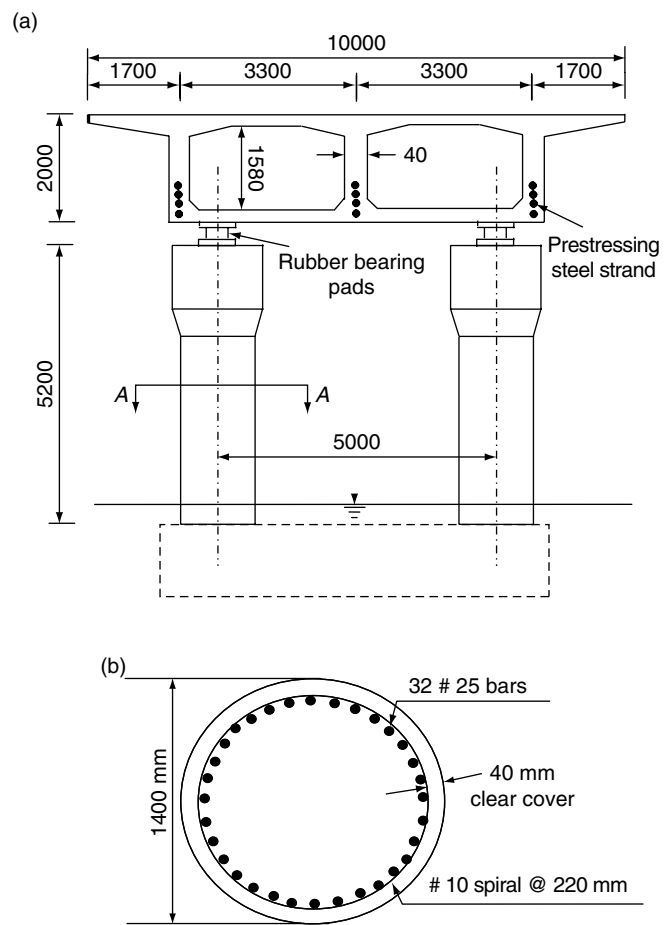

Figure 3. (a) Cross section of the bridge at the pier centre; and (b) Cross section of the bridge column

Table 1. The parameters of the girder and pier

Parameter of bridge girder		Parameter of bridge pier	
Length of span	$x_0 = 38$ m	Height of pier	$L = 5.2$ m
Mass density	$\rho = 2600$ kg/m^3	Mass density	$\rho = 2600$ kg/m^3
Cross-section area	$A_c = 6.06$ m^2	Cross-section area	$A_c = 3.0772$ m^2
Young's modulus of concrete	$E_c = 34.5$ GPa	Young's modulus of concrete	$E_c = 30.0$ GPa
Inertia moment of girder cross section	$I_c = 3.409$ m^4	Reinforcement cross section area	$A_y = 0.0157$ m^2
Reinforcement cross section area	$A_y = 0.04712$ m^2	Young's modulus of reinforcement	$E_y = 200$ GPa
Young's modulus of reinforcement	$E_y = 200$ GPa		
Inertia moment of reinforcement cross section	$I_y = 0.1925$ m^4		
Prestressed steel strand section area	$A_p = 0.02688$ m^2		
Young's modulus of prestressed steel strand	$E_p = 195$ GPa		
Inertia moment of prestressed steel strand cross section	$I_p = 0.07585$ m^4		

5. NUMERICAL RESULTS

5.1. Effect of Vertical Earthquake Ground Motion on Bridge Bearing

To investigate the effect of vertical earthquake ground motion on bridge structures, responses of the bridge model under the three recorded vertical ground displacements are calculated using the above derived analytical solutions. Figures 5, 6 and 7 show the time history of the reaction force on the bearing, the vertical displacement time histories at the middle of the girder (point O in Figure 2) and at the pier top (point C in Figure 2) under Kobe earthquake, Northridge earthquake and Imperial Valley earthquake, respectively.

As show in Figure 5, no vertical pounding occurs when this bridge is subjected to the Kobe earthquake. This is because, as shown in Figure 5(b), displacement at point O is always less than that at the pier top, implying the girder is always in contact with the bearing throughout the entire earthquake duration. The reaction force provided by the bearing is not constant because of the vertical earthquake loading. As shown in Figure 5(a), the maximum and minimum of the reaction forces are 15.78 MN and 7.35 MN, respectively.

Figure 6 shows that when the bridge is subjected to the Northridge earthquake, the displacement at the pier top becomes smaller than that at the middle of the girder at 6.26 sec, indicating separation of the girder from the bearing occurs, and therefore the axial force in the bearing is zero. The first separation phase starts to take place and bridge girder and pier vibrates independently before they are in contact again. The bridge girder will be in contact again with the bearing and induce a relatively large impact force on bearing as shown in Figure 6(a). As shown in Figure 6, the separation and impacting process repeats several times after 6.26 sec, indicating multiple vertical poundings take place. It also can be seen that the maximum reaction force acted on the bearing is 64.5 MN, which is about three times of the axial force of about 20 MN in the bearing if there is no vertical pounding, indicating quite severe vertical pounding effect. The maximum up throwing of the middle of the girder, i.e., the largest separation between the girder and bearing is 70.9 mm, occurring at about 7.5 sec.

When the bridge is subjected to Imperial Valley earthquake, only single separation and thus one pounding takes place as shown in Figure 7. The

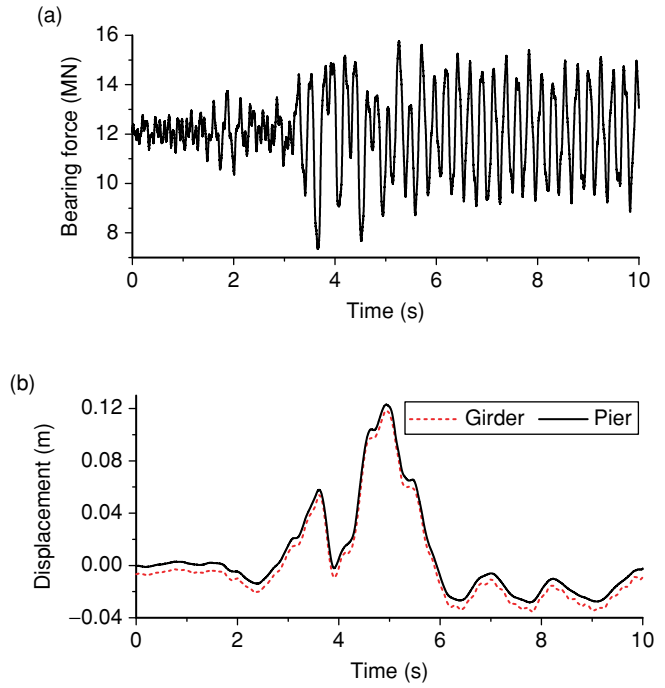**Table 2. Basic information of selected vertical ground motions**

| Number	Earthquake	Year	Station	M_W	Distance (km)	PGA (g)	PGV (cm/s)	PGD (cm)
1	Kobe, Japan	1995	Takarazuka	6.9	1.2	0.433	34.8	12.38
2	Northridge	1994	Tarzana-Cedar Hill A	6.7	4.1	1.048	75.4	20.05
3	Imperial Valley	1979	EI Centro Array #8	6.5	1.0	1.655	57.5	26.41

(a)

(b)

(c)
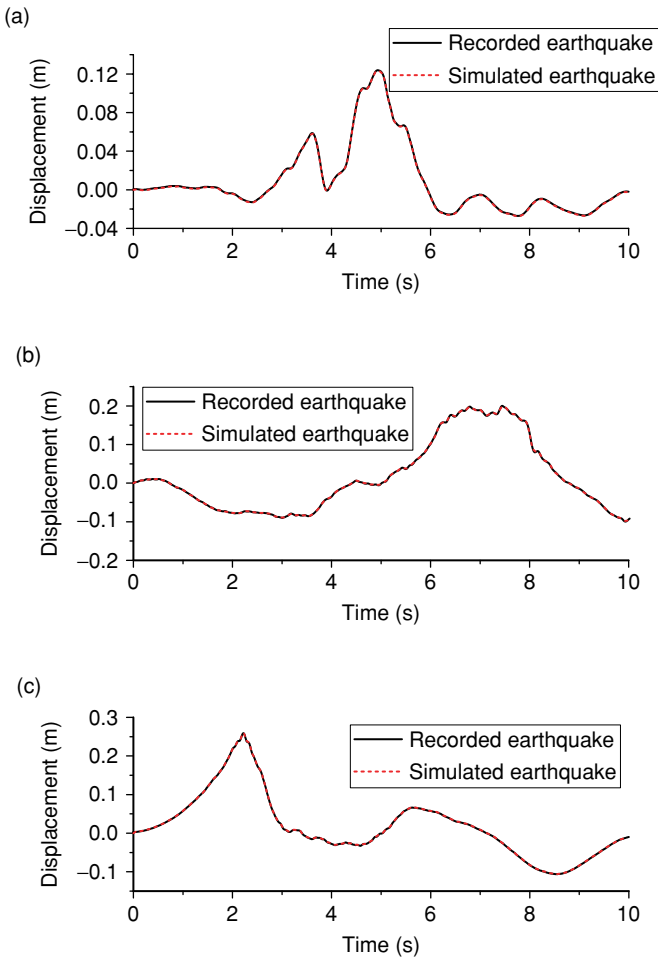
Figure 4. Simulated and recorded vertical earthquake ground displacement time histories: (a) Kobe earthquake; (b) Northridge earthquake; and (c) Imperial Valley earthquake
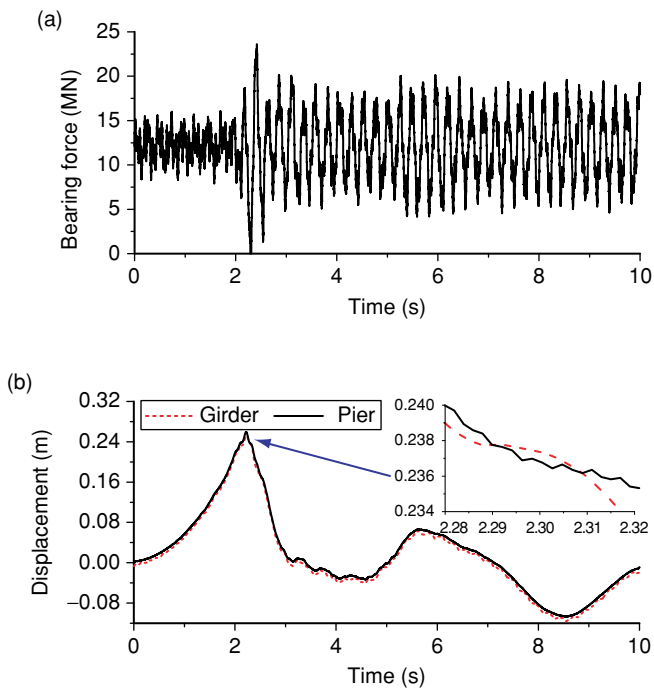

Figure 5. Seismic response time histories of the bridge model to Kobe earthquake: (a) bearing force; and (b) vertical displacement of the girder above the bearing and pier top
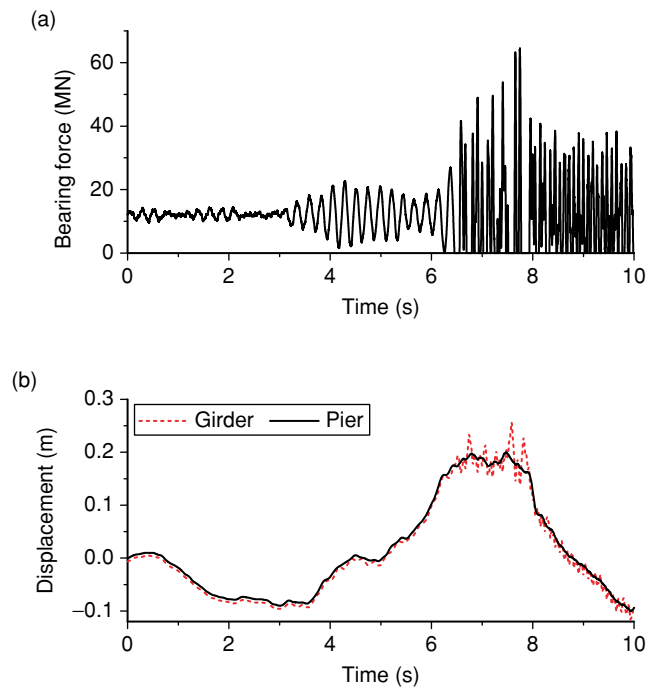
Figure 6. Seismic response time histories of the bridge model to Northridge earthquake: (a) bearing force; and (b) vertical displacement of the girder above the bearing and the pier top

separation occurs at 2.29 sec, and at 2.31 sec, the girder falls back on the rubber bearing, inducing a relatively large pounding force of 23.6 MN in the bearing.

It should be noted that the PGA and peak ground displacement (PGD) of the Imperial Valley earthquake is much larger than those of the Northridge earthquake as shown in Table 1 and Figure 4. However, Northridge earthquake induces multiple vertical poundings while the larger amplitude Imperial Valley earthquake causes only a single vertical pounding. This is because the frequency of the vertical impulse from the Imperial Valley earthquake is higher and the ground displacement quickly changes direction, as compared to that of the Northridge earthquake, as shown in Figure 4. The large impulse in the vertical ground displacement of the Northridge earthquake lasts almost 2.0 sec, therefore resulting in multiple vertical poundings. These numerical results indicate that the vertical structural response not only depends on the ground motion amplitude, but also on ground

motion frequency and duration, as well as structural characteristics. The most server earthquake not

Figure 7. Seismic response time histories of the bridge model to Imperial Valley earthquake: (a) bearing force; and (b) vertical displacement of the girder above the bearing and the pier top

necessarily results in the most serious damage to engineering structures.

The above numerical results demonstrate that under strong vertical ground excitations, bridge girder might separate from the supporting bearing and vertical poundings may take place. Although the girder only separates from the bearing in a very short period with small a gap, the pounding force it generates could be rather large when the girder falls back in contact again with the bearing. The above numerical results show that the axial force in the bearing due to pounding is about three times larger than that without pounding. Such a large impact force can lead to the fracture of bearing and local damage of bridge girder and pier. For example, Tanimura *et al.* (2002) identified that the vertical poundings between the girder and the bearing lead to the fracture of the bearing in Nielsen Bridge. Vertical pounding damages to piers of a few bridges were also observed in the 2011 Christchurch earthquake, including the Durham Street Bridge and ANZAC Drive Bridge (Chouw and Hao 2012). Therefore it is important to take vertical ground vibration into consideration in bridge structural response analysis.

5.2. Effect of Vertical Earthquake Ground Motion on the Bridge Girder

To investigate the effect of vertical earthquake ground

motion on the bridge girder, the responses of the girder to the above three vertical earthquake ground motions are calculated. Figures 8, 9 and 10 show the response time histories of the bending moment at mid-span and at the bearing support location (Point O in Figure 2) under Kobe earthquake, Northridge earthquake and Imperial Valley earthquake, respectively.

As shown in Figure 5, when the bridge is under Kobe earthquake, no vertical pounding takes place. Therefore the bending moment response is rather steady and follows the amplitude of ground vibration, as shown in Figure 8. The maximum of bending moment is 32.4 MN·m. Similar observations can also be made for the negative bending moment as shown in Figure 8(b). When the bridge is subjected to the Northridge earthquake, multiple poundings take place as discussed above. The vertical poundings also affect the bending moments in the girder as shown in Figure 9. As shown the amplitude of the positive bending moment at the mid span quickly increases after 6.26 sec owing to vertical poundings. The maximum positive moment reaches 109.7 MN·m, which is substantially higher than the bending moment before pounding occurs. Similar observations can also be made on the negative moment response as shown in Figure 9(b). The maximum negative moment is 158.6 MN·m. When the bridge is subjected to the Imperial Valley earthquake, only one pounding takes place. The pounding also causes a sudden increase in the bending moments. The maximum positive and negative bending moments are 48.04 and 88.5 MN·m respectively.

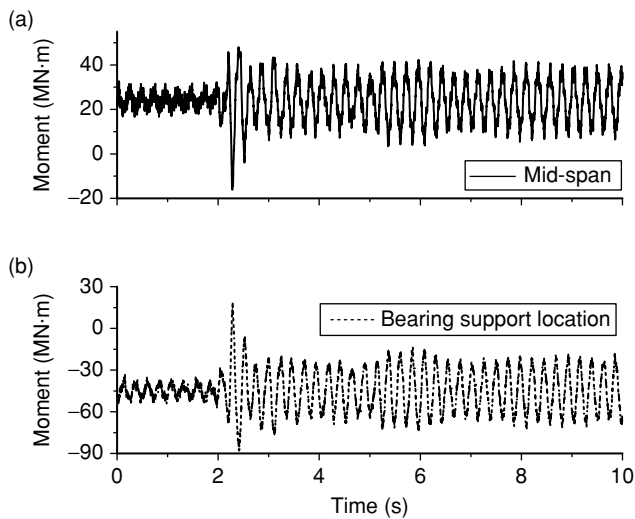To further investigate the influences of vertical
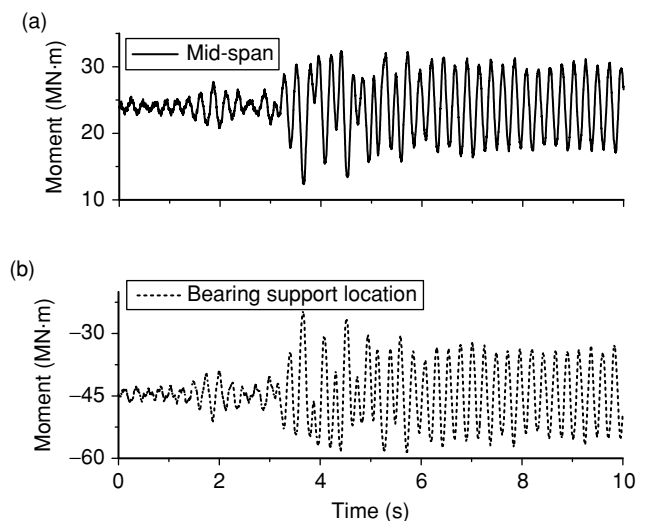
Figure 8. The moment responses of girder under Kobe earthquake: (a) the positive moment at mid-span; and (b) the negative moment at bearing support location

(a)

(b)
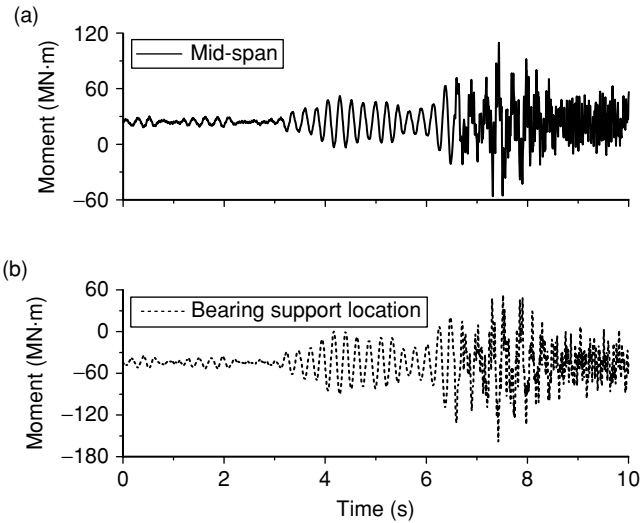
Figure 9. The moment responses of girder under Northridge earthquake: (a) the positive moment at mid-span; and (b) the negative moment at bearing support location

(a)

(b)

Figure 10. The moment responses of girder under Imperial Valley earthquake: (a) the positive moment at mid-span; and (b) the negative moment at bearing support location

pounding on bending moment responses of the bridge girder, Figure 11 shows the bending moment of bridge girder at different time instants near the separation and pounding occurrence. The horizontal axis $\bar{x} = x/x_0$ is the normalized distance measured from the point directly above the bearing. The girder is separated from the bearing in the period of 2.29 sec to 2.31 sec, and the maximum pounding force appears at 2.42 sec as shown in Figure 7. Figure 11 shows that pounding results in a sharp increase in the bending moment response in the girder (comparing those at the time instant 2.31 sec, to

2.35 sec and 2.42 sec). The bending moments at mid-span change from −13.8 MN·m to 49.97 MN·m and those at bearing support location change from −87.5 MN·m to 14.42 MN·m. These observation indicate that when pounding occurs, the bending moments in the bridge girder may fluctuate suddenly, and the the initial positive moment at mid-span may become negative and the initial negative moment at bearing support location may become positive. This sudden fluctuation may cause serious damage to the bridge girder. Since most bridge girders are designed to resist positive bending moment at the mid-span and negative bending moment above the pier due to gravity load, and the reinforcement bars are placed accordingly, vertical pounding induced bending moments might lead to damages to the bridge girder if they are not properly accounted for in the design and analysis.

5.3. Effect of Vertical Earthquake Ground Motion on the Bridge Pier

To investigate the effect of vertical earthquake ground motion on the pier response, axial responses of the bridge pier is also calculated. Figure 12 shows the time histories of the axial stress at the bottom of the pier under Kobe earthquake, Northridge earthquake and Imperial Valley earthquake, respectively.

Similar to the bending moments in Section 5.2, under Kobe earthquake the variations of the axial stress is relatively low as shown in Figure 12(a), and only the compressive stress develops in the pier because this earthquake ground motion does not induce vertical pounding. However, when pounding occurs, large axial stress could be generated in the pier owing to the vertical pounding force. It is interesting to note that tensile axial stress may also develop in the pier as shown
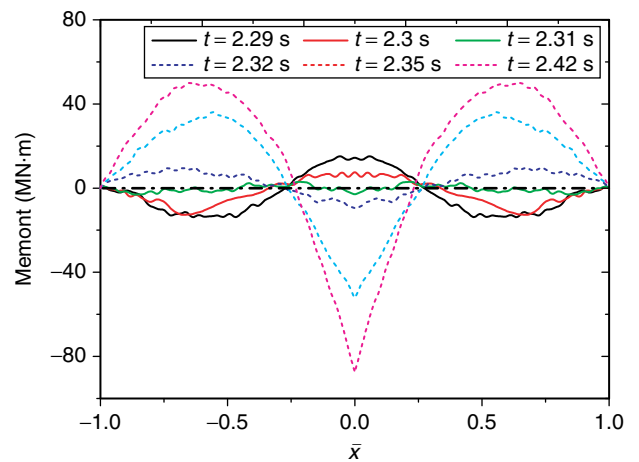
Figure 11. The bending moment distribution along the girder at different time instants under Imperial Valley earthquake

in Figures 12(b) and (c). This is because lifting up of the girder from the bearing results in zero compressive force acting on the pier besides the pier self-weight. Reflection of the stress wave at the bottom of the pier, if larger than the compressive stress due to self-weight, therefore generates tensile stress. As shown in Figure 12(c), wave reflection may generate tensile stress at the bottom of the pier even the bridge girder does not completely separate from the bearing but the vertical vibration results in the compressive stress from the bridge girder on the pier relatively small. To examine in more detail the axial stress fluctuations and the tensile stress induced by vertical earthquake and pounding, responses of the pier to the Imperial Valley earthquake is taken as the example again. Figure 13 shows the axial stress of the pier at different time instants close to the instants when separation and pounding occur. The

horizontal axis $\bar{\xi} = \xi/L$ is the normalized pier height. As shown in Figure 13, at $t = 2.29$ sec when the girder begins to separate from the bearing, most positions along the pier are in compression owing to the combined actions of pier self-weight and stress wave inside the pier generated from the vertical vibrations, except at the top portion of the pier, where the stress is almost zero. At 2.295 sec, some positions begin to experience tensile stress and the tensile zone and compression zone oscillates owing to stress wave propagation along the pier. At 2.3 and 2.305 sec, the whole pier is in tension, and the maximum tensile stress can reach 2.4 MPa as shown in Figure 13. This tensile stress may result in the annular cracks on concrete bridge pier as observed in many previous major earthquakes. At 2.31 sec, the girder drops back to the bearing again, the upper part of the pier becomes in compression again, but the lower part is still in tension. At 2.35 sec, the whole pier becomes to be in compression again. At 2.41 sec, the axial stress rapidly increases to 8 MPa. Under Northridge earthquake the maximum of compressive stress is more than 20 MPa because of vertical pounding, about four times larger than the compressive stress in the pier from the static vertical loads, implying the vertical poundings may induce crushing failure of concrete pier or buckling failure of steel pier if they are large enough, such failure modes of bridge pier have in fact been observed in previous earthquakes.

6. CONCLUSIONS
This paper derives the theoretical solutions of the vertical pounding responses between bridge girder and supporting bearing of a continuous bridge structure subjected to strong near-fault vertical earthquake
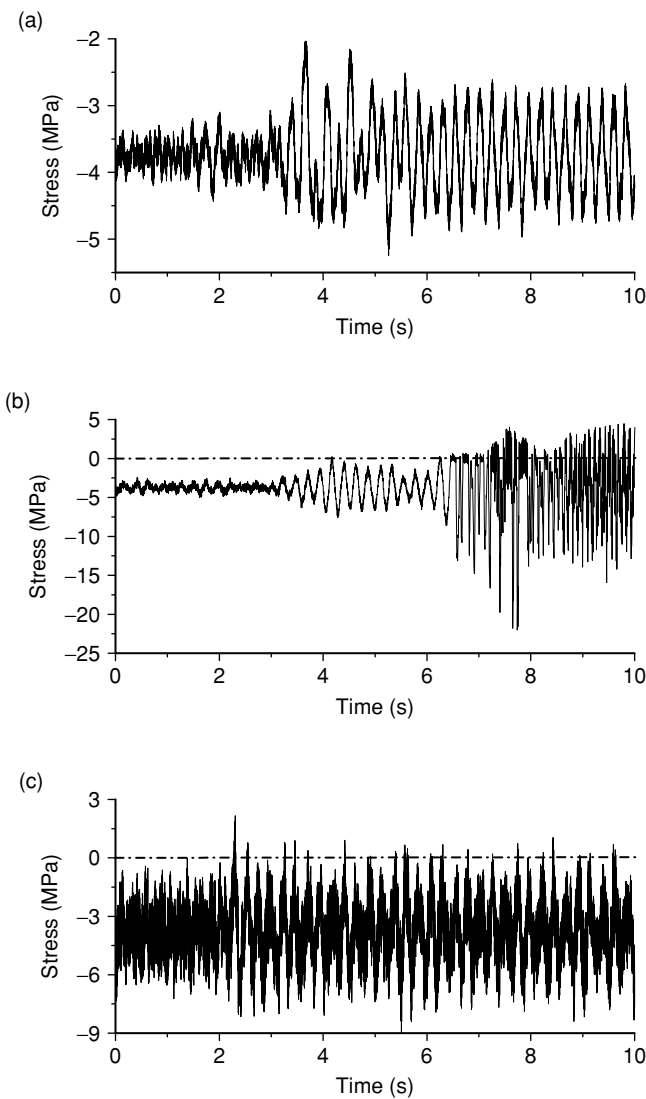

Figure 12. Axial stress responses at the pier: (a) Kobe earthquake; (b) Northridge earthquake; and (c) Imperial Valley earthquake
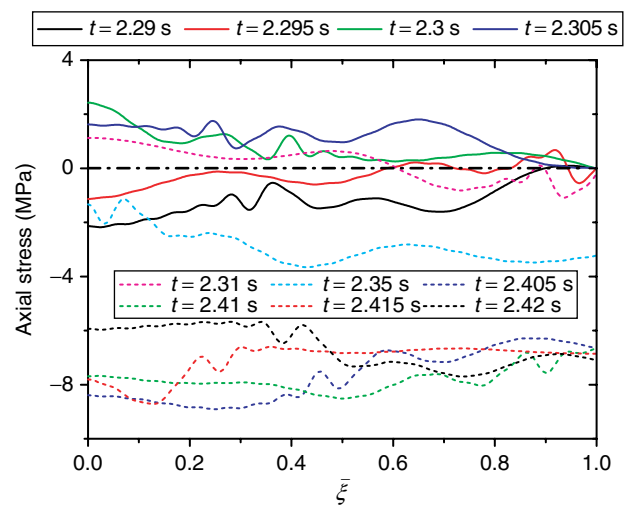

Figure 13. The Axial stress distribution along the pier at different time instants under Imperial Valley earthquake

ground excitations, and investigates the influences of vertical poundings on bridge structure responses. The bridge is simplified as a continuous beam with pin supports at the two abutments, and a compression-only spring connecting the beam and the bridge pier. The separation of the bridge girder from the bearing due to strong vertical excitation and its pounding on the bearing after it is in contact again with the bearing are modelled. By using the expansion of transient wave functions as a series of Eigenfunctions, the theoretical solutions of the seismic responses of the bridge with vertical separation and pounding at the bearing-girder connection under near-fault vertical ground excitation are derived. The effects of vertical earthquake ground excitation and vertical pounding on bridge bearing, girder and pier are then investigated. Following conclusions are obtained based on the numerical results:

1. Vertical pounding between the bridge girder and the supporting bearing may take place when the bridge structure is subjected to severe near-fault earthquake. The occurrence of separation and pounding between the bridge girder and bearing depends not only on the vertical ground motion amplitude, but also on its frequency, duration and the structure characteristics.

2. Under strong vertical ground excitations, separation of girder from bearing and hence pounding on the bearing by the girder is possible. Such vertical pounding generates a large impact force on the bearing, and may lead to the fracture of bearing and local damage to the bridge pier.

3. The vertical poundings between the bridge girder and the bearing may result in large bending moments in the bridge girder, and these bending moments are in the opposite direction of those from static and traffic loading, and therefore are not necessarily appropriately accounted for since vertical pounding is not considered in normal bridge designs.

4. The vertical pounding may also increase the compressive axial stress in the bridge pier and cause tensile axial stress owing to stress wave reflection. The excessive compressive and tensile axial stress may cause crushing/buckling damage or lead to annular cracks in the pier.

ACKNOWLEDGEMENTS

REFERENCES

Bi, K. and Hao, H. (2013). "Numerical simulation of pounding damage to bridge structures under spatially varying ground motions", *Engineering Structures*, Vol. 46, No. 1, pp. 62−76.

Bi, K., Hao, H. and Chouw, N. (2010). "Required separation distance between decks and at abutments of a bridge crossing a canyon site to avoid seismic pounding", *Earthquake Engineering and Structural Dynamics*, Vol. 39, No. 3, pp. 303−323.

Bi, K., Hao, H. and Chouw, N. (2011). "Influence of ground motion spatial variation, site condition and SSI on the required separation distances of bridge structures to avoid seismic pounding", *Earthquake Engineering and Structural Dynamics*, Vol. 40, No. 9, pp. 1027−1043.

Bi, K., Hao, H. and Chouw, N. (2013). "3D FEM analysis of pounding response of bridge structures at a canyon site to spatially varying ground motions", *Advances in Structural Engineering*, Vol. 16, No. 4, pp. 619−640.

Bozorgnia, Y. and Campbell, K.W. (1995). "The vertical-to-horizontal response spectral ratio and tentative procedures for developing simplified V/H and vertical design spectra", *Journal of Earthquake Engineering*, Vol. 8, No. 2, pp. 175−207.

Button, M.R., Cronin, C.J. and Mayes, R.L. (2006). "Effect of vertical motions on seismic response of highway bridges", *Journal of Structural Engineering*, ASCE, Vol. 128, No. 12, pp. 1551−1564.

Colloer, C.J. and Elnashai, A.S. (2001). "A procedure for combining vertical and horizontal seismic action effects", *Journal of Earthquake Engineering*, Vol. 5, No. 4, pp. 521−539.

Chouw, N. and Hao, H. (2011). "Pounding damage to buildings and bridges in the 22 February 2011 Christchurch Earthquake", *International Journal of Protective Structures*, Vol. 3, No. 2, pp. 123−139.

Elnashai, A.S. and Papazoglou, A.J. (2001). "Procedure and spectra for analysis of RC structures subjected to strong vertical earthquake loads", *Journal of Earthquake Engineering*, Vol. 1, No. 1, pp. 121-155.

Gulerce, Z., Erduranm, E., Kunnath, S.K. and Abrahamson, N.A. (2012). "Seismic demand models for probabilistic risk analysis of near fault vertical ground motion effects on ordinary highway bridges", *Earthquake Engineering and Structural Dynamics*, Vol. 41, No. 2, pp. 159−175.

Jonsson, M.H., Bessason, B. and Haflidason, E. (2010). "Earthquake response of a base-isolated bridge subjected to strong near-fault ground motion", *Soil Dynamics and Earthquake Engineering*, Vol. 30, No. 6, pp. 447−455.

Kim, S.J., Holub, C.J. and Elnashai, A.S. (2011). "Analytical assessment of the effect of vertical earthquake motion on RC bridge piers", *Journal of Structural Engineering*, ASCE, Vol. 137, No. 2, pp. 252−260.

Kim, S.J., Holub, C.J. and Elnashai, A.S. (2011). "Experimental investigation of the behavior of RC bridge piers subjected to horizontal and vertical earthquake motion", *Engineering Structures*, Vol. 33, No. 7, pp. 2221−2235.

Kunnath, S.K., Erduran, E., Chai, Y.H. and Yashinsky, M. (2008). "Effect of near-fault vertical ground motions on seismic response of highway overcrossings", *Bridge Engineering*, Vol. 13, No. 3, pp. 282−290.

Lee, H. and Mosalam, K.M. (2014). "Seismic evaluation of the shear behavior in reinforced concrete bridge columns including effect of vertical accelerations", *Earthquake Engineering and Structural Dynamics*, Vol. 43, No. 2, pp. 317−337.

Legeron, F. and Sheikh, M.N. (2009). "Bridge support elastic reactions under vertical earthquake ground motion", *Engineering Structures*, Vol. 31, No. 10, pp. 2317−2326.

Pant, D.R. and Wijeyewickrema, A.C. (2013). "Influence of near-fault ground motions on the response of base-isolated reinforced concrete buildings considering seismic pounding", *Advances in Structural Engineering*, Vol. 16, No. 12, pp. 1973−1988.

Papazoglou, A.J. and Elnashai, A.S. (1996). "Analytical and field evidence of the damaging effect of vertical earthquake ground motion", *Earthquake Engineering and Structural Dynamics*, Vol. 25, No. 10, pp. 1109−1137.

Saadeghvaziri, M.A. and Foutch, D.A. (1991). "Dynamic behavior of RC highway bridge under the combined effect of vertical and horizontal earthquake motions", *Earthquake Engineering and Structural Dynamics*, Vol. 20, No. 6, pp. 535−549.

Tanimura, S., Sato, T., Umeda, T., Mimura, K. and Yoshikawa, O. (2002). "A note on dynamic fracture of the bridge bearing due to the great Hanshin-Awaji earthquake", *International Journal of Impact Engineering*, Vol. 27, No. 2, pp. 153−160.

Wang, C. and Kim, J. (1996). "New analysis method for a thin beam impacting against a stop based on the full continuous model", *International Journal of sound and Vibration*, Vol. 191, No. 5, pp. 809−823.

Wang, D. and Xie, L. (2009). "Attenuation of peak ground accelerations from the great Wenchuan earthquake", *Earthquake Engineering and Engineering Vibration*, Vol. 8, No. 2, pp. 179−188.

Wang, G.Q., Zhou, X.Y., Zhang, P.Z. and Igel, H. (2010). "Characteristics of amplitude and duration for near fault strong ground motion from the 1999 Chi-Chi, Taiwan earthquake", *Soil Dynamics and Earthquake Engineering*, Vol. 22, No. 1, pp. 73−96.

Yang, J. and Lee, C.M. (2007). "Characteristics of vertical and horizontal ground motions recorded during the Niigata-ken Chuetsu, Japan Earthquake of 23 October 2004", *Engineering Geology*, Vol. 94, No. 1−2, pp. 50−64.

Yin, X.C. (1997). "Multiple impacts of two concentric hollow cylinders with zero clearance", *International Journal of Solids and Structures*, Vol. 34, No. 35−36, pp. 4597−4616.

Yin, X.C., Qin, Y. and Zou, H. (2007). "Transient responses of repeated impact of a beam against a stop", *International Journal of Solids and Structures*, Vol. 44, No. 22−23, pp. 7323−7399.

Yin, X.C. and Wang, L.G. (1999). "The effect of multiple impacts on the dynamics of an impact system", *International Journal of Sound and Vibration*, Vol. 228, No. 5, pp. 995−1015.

Yin, X.C. and Yue, Z.Q. (2002). "Transient plane-strain response of multilayered elastic cylinders to axisymmetric impulse", *Journal of Applied Mechanics*, Vol. 69, No. 6, pp. 826−835.

Yu, C.P. (1996) "Effect of vertical earthquake components on bridge responses", PhD Thesis, University of Texas at Austin, Texas, USA.